Journal of Materials Chemistry A

Tellurene based Chemical Sensor

Journal:	*Journal of Materials Chemistry A*
Manuscript ID	TA-ART-08-2019-009429.R2
Article Type:	Paper
Date Submitted by the Author:	21-Oct-2019
Complete List of Authors:	Wang, Dawei; Xi'an Jiaotong University Yang, Aijun; Xi'an Jiaotong University Lan, Tiansong; Xi'an Jiaotong University Fan, Chengyu; Xi'an Jiaotong University Pan, Jianbin; Xi'an Jiaotong University Liu, Zhu; Xi'an Jiaotong University Chu, Jifeng; Xi'an Jiaotong University, State Key Laboratory of Electrical Insulation and Power Equipment Yuan, Huan; Xi'an Jiaotong University Wang, Xiaohua; Xi'an Jiaotong University Rong, Mingzhe; Xi'an Jiaotong University Koratkar, Nikhil; Rensselaer Polytechnic Institute

ARTICLE

Tellurene based Chemical Sensor

Dawei Wang[a †], Aijun Yang[a †], Tiansong Lan[a †], Chengyu Fan[a], Jianbin Pan [a], Zhu Liu[a], Jifeng Chu[a], Huan Yuan[a], Xiaohua Wang[a, *], Mingzhe Rong[a, *] and Nikhil Koratkar[b,c*]

Received 00th January 20xx,
Accepted 00th January 20xx

DOI: 10.1039/x0xx00000x

Chemiresistive sensor devices using two-dimensional (2D) materials have been extensively studied. However, so far no single material has all the desirable attributes. For example, graphene and MXenes lack a band gap, transition metal dichalcogenides (such as MoS_2) lack high sensitivity, while phosphorene exhibits poor air-stability. Here we report that tellurene, a new emergent single-element 2D material, excels as a sensor for NO_2 detection. Devices based on tellurene exhibit a detection limit of ~25 ppb, large detection range (from 25 ppb to 5 ppm), baseline noise as low as ~0.5%, and excellent "selectivity" to NO_2 even in the presence of cross-contaminants such as CO, SO_2, H_2S, acetone and ethanol. Density functional theory calculations indicate that large adsorption energy and intense charge redistribution are the reasons for the high sensitivity and selectivity of tellurene for NO_2 detection. Further, we find that "heat-pulsing" enables fast sensor response and recovery time, without damaging the tellurene sheets. Most importantly, tellurene exhibits outstanding air-stability, making it a promising candidate for next-generation chemical sensors.

Introduction

Since the successful synthesis of graphene, 2D materials have opened up a Pandora's box of new fundamental science as well as important technological applications.[1-9] For example, graphene was reported to have the ability to resolve the adsorption of an individual gas molecule, leading to ultra-sensitive chemical sensors.[1] After graphene, other emerging 2D materials such as phosphorene (single-element 2D materials), MoS_2 (transition-metal sulfides, TMDC), and $Ti_3C_2T_x$ (MXene) were synthesized and explored for gas sensing applications.[10-13] Compared with traditional metal oxide gas sensors, 2D materials offer enhanced sensitivity, possibility for room temperature operation and low power consumption.[14-19]

However, there are several key limitations that hinder the development of 2D materials for chemical sensing. For graphene and MXene, it is the lack of a band gap.[13, 20] The sensitivity of MoS_2 needs improvement[12], while phosphorene is highly sensitive but lacks air-stability and ages rapidly when exposed to the ambient.[20] Recently, tellurene - a new single-element 2D material - has been successfully synthesized by different routes.[21-27] Tellurene has many attractive features, which include: high room-temperature carrier mobility, superior on-state current density, process-tunable bandgap and excellent air-stability, which has generated immense interest and excitement in the use of this material in electronic and optoelectronic device applications.[22] In addition, 2D tellurene has a puckered lattice configuration which is similar to phosphorene. The puckered structure provides tellurium atoms in different coordination environments on the surface which would be a big advantage for sensing.[24] In spite of these promising features, there is no experimental study to date that has investigated the performance of tellurene as a chemical sensor.

In this work, we systematically studied the chemical sensing performance (limit of detection, sensitivity, selectivity, baseline noise, repeatability, and baseline drift) of tellurene for the detection of nitrogen dioxide (NO_2), which is a highly toxic industrial pollutant. Our tests reveal that tellurene excels as a NO_2 sensing material. The limit of detection (LOD) is as low as ~25 parts per billion (ppb) toward NO_2 in N_2 that is comparable with the sensitivity of phosphorene based sensors.[11] The baseline noise is as low as ~0.5%, which is much lower than that of typical 2D materials with a band gap such as phosphorene and MoS_2.[13] The very high "selectivity" of tellurene towards NO_2 detection was also verified in our experiments. In particular, we found that other common industrial contaminants (such as CO, SO_2, H_2S, NH_3, acetone and ethanol) had a much weaker impact on the tellurene sensor response when compared to NO_2. Finally, a major drawback of 2D materials – their long recovery

[a.] State Key Laboratory of Electrical Insulation for Power Equipment, Xi'an Jiaotong University, Xi'an 710049, PR China
[b.] Department of Mechanical, Aerospace and Nuclear Engineering, Rensselaer Polytechnic Institute, Troy, NY 12180, USA
[c.] Department of Materials Science and Engineering, Rensselaer Polytechnic Institute, Troy, NY 12180, USA
† These authors contributed equally to this work.
Electronic Supplementary Information (ESI) available: Experimental details, more characterization images, and DFT calculation. See DOI:

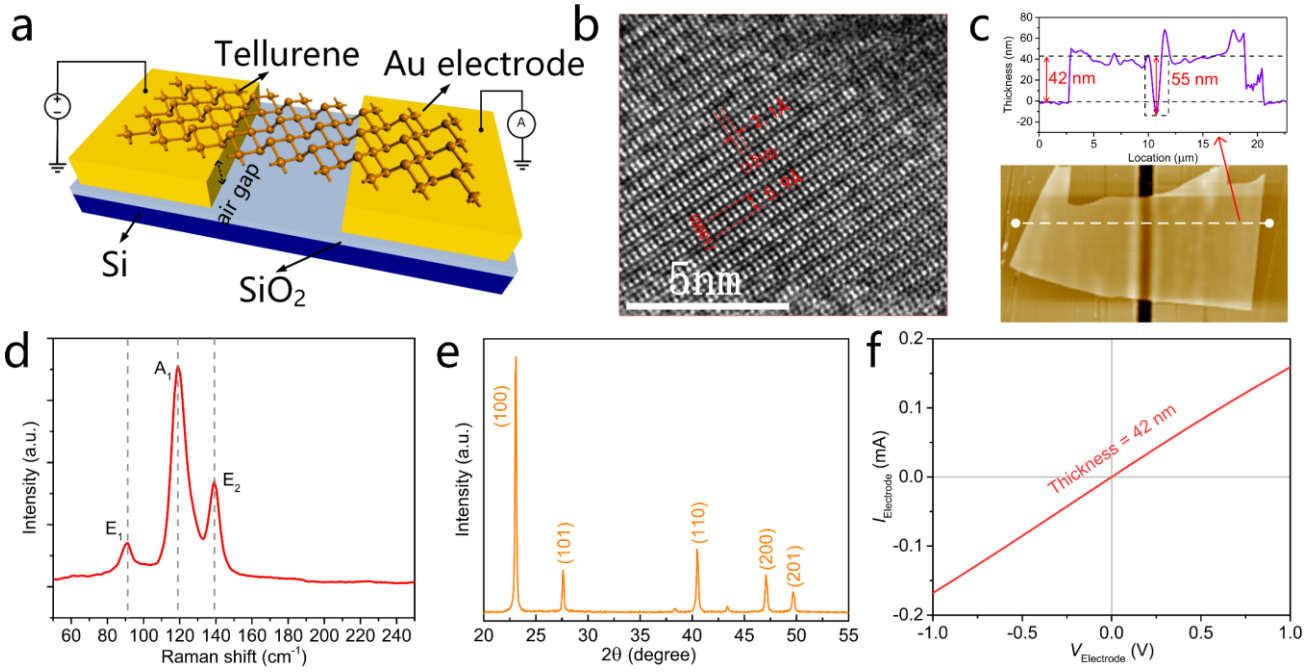

Fig. 1 Schematic and morphological characterization of tellurene based sensors. **a**. Schematic of the sensor device. **b**. High resolution transmission electron microscope (HRTEM) image of tellurene flakes. **c**. Atomic force microscope (AFM) image of the tellurene flake. **d**. X-ray diffractometer (XRD) patterns of the tellurene flake. **e**. Raman spectra of tellurene (E_1 at 91.4 cm^{-1}, A_1 at 119.0 cm^{-1}, and E_2 at 139.2 cm^{-1}). **f**. Current-voltage (*I-V*) response directly measured on the tellurene sensor via a two-terminal method.

times was also successfully overcome by the application of heat pulses. Ab initio calculations were also performed to understand the underlying mechanism(s) that are responsible for tellurene's superior performance. These calculations indicate that the high sensitivity and selectivity of tellurene can be attributed to the higher adsorption energy and more intense charge redistribution induced by NO_2 adsorption when compared to those of other common pollutants such as CO and SO_2. In particular, the excellent air-stability of tellurene sets it apart from other competing 2D materials such as phosphorene, whose air-stability is poor. The above attributes make tellurene particularly promising, as a next-generation gas sensing material.

Experimental section

Materials synthesis

All reagents used in the experiments were analytically pure without further purification and purchased from Sinopharm Chemical Reagent Co., Ltd. (Shanghai, China). The tellurene flakes are synthesized by a facile one-step hydrothermal route[20]. In a typical procedure, ~100 mg of Na_2TeO_3 and ~345 mg of Polyvinyl Pyrrolidone (PVP, k17) were placed into deionized water (~33 ml) with magnetic stirring at room temperature for ~10 min. Then the solution was mixed with ~1ml hydrazine hydrate (85%, wt/wt%) and ~2 ml aqueous ammonia solution (~25%, wt/wt%). The above mixture was transferred into a ~50 ml Tefon-lined stainless-steel autoclave to react at ~180° C for ~40 h. The resulting solid silver-grey products were washed five times by the suction filtration method (bore diameter: 5 μm) to remove any ions remaining in the final product. The as-synthesized tellurene solution (~1 ml) was mixed with acetone (~3 ml) at temperature for ~1 h to remove PVP molecules adsorbed on tellurene surface. Finally, the resulting solution was washed three times with deionized water by the suction filtration method.

Characterization of materials

Tellurene was synthesized by a facile hydrothermal approach.[21, 26] The optical image and transmission electron microscope (TEM) image of as-synthesized tellurene flakes are displayed in **Figure S1-S2**. The typical thickness of the tellurene is in the range of 30 to 80 nm and the typical width is between 5 and 50 μm. To establish tellurene in the device channel (**Figure 1a**), tellurene fakes were first transferred to polydimethylsiloxane (PDMS) followed by transfer of the multilayer tellurene to the fabricated electrodes by the aligned transfer method.[29] It should be noted that this constitutes an all-dry transfer. Compared with chemical etching based approaches, all-dry transfer avoids the possibility of contamination during the transfer process, resulting in a clean surface. Additional details regarding device fabrication are described in the Methods Section. The electrodes were fabricated on highly doped silicon wafers with ~300 nm thermally oxidized SiO_2 dielectric layers (**Figure S3**). Projection lithography was employed and the gap of subtle line is ~1 μm. The thickness of the metal contact (Cr/Au) is about 180 nm. The tellurene is transferred to the upper surface of the contact, so that a suspended structure is formed as shown in **Figure 1a**. The air gap between the tellurene sheet and the substrate is ~80 nm, as indicated by the

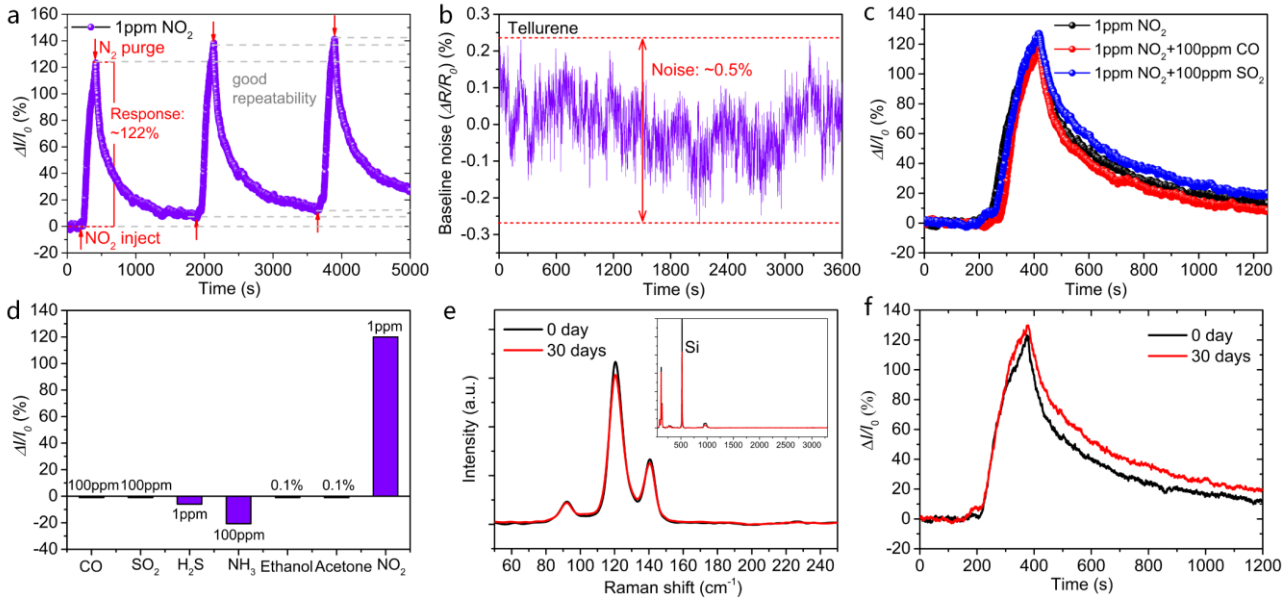

Fig. 2 NO_2 gas-sensing properties of the tellurene sensor: **a**. Time dependent gas-sensing response toward ~1 ppm NO_2; **b**. Baseline noise of the tellurene sensor device; **c**. Dynamic sensing response curve towards ~1 ppm NO_2 mixed with ~100 ppm CO and ~100 ppm SO_2; **d**. Response value of the tellurene sensor towards CO, SO_2, H_2S, NH_3, ethanol, acetone, and NO_2. **e**. Raman spectra indicating the stability of tellurene when exposed to air (at ~25°C and ~50% relative humidity); **f**. Dynamic response of the sensor device to ~1 ppm NO_2 showing no significant change even after continuous exposure to air (at ~25°C and ~50% relative humidity) for a 30 days period.

AFM measurement in **Figure 1c**. Such a suspended structure is important since it minimizes doping effects induced by contact with the substrate and increases the exposed surface area of the tellurene structure, which is important to maximize the device sensitivity.[30] Additional microscopy and spectroscopy characterization of the tellurene sheets is provided in **Figure 1b-e**. The high resolution transmission electron microscope (HRTEM) image of tellurene flakes demonstrated the crystal parameters of tellurene, which is consist with the previous result.[21] The thickness of the tellurene flake was characterized by atomic force microscope (AFM) and was measured at ~42 nm. The crystalline properties of tellurene were characterized by X-ray diffraction (XRD) measurement. The XRD pattern is consistent with previous work, which has successfully synthesized tellurene.[26] The corresponding Raman spectra is shown in **Figure 1e**. Three active modes located at ~91.4 cm^{-1} (E_1 mode), ~119.0 cm^{-1} (A_1 mode) and ~139.2 cm^{-1} (E_2 mode) were identified, which is also consistent with previous work.[21] A two-terminal current-voltage (*I-V*) measurement was performed to elucidate the contact condition of tellurene and the electrode. The linear *I-V* curve indicates that an ohmic contact was successfully established with the tellurene flake.

Gas delivery system and current measurement

A schematic diagram of the gas sensor testing system is shown in **Figure S3**. The fabricated sensors were loaded inside a homemade gas sensing chamber (Volume: ~50 ml). The testing gases (NO_2, CO, and SO_2) used in this study were N_2 based 5-200 ppm gases. Mass flow controllers (MFC, SevenStar) were used to control the flow rate of gas. The current measurement was performed using a semiconductor analyzer (Keithley 2612B). The bias voltage was set to 50 mV all the time. The response was defined as the relative current change $\Delta I/I_0$ (where $\Delta I = I - I_0$, I is the instantaneous conductance of the device, and I_0 is the conductance of the device before exposure to target gases).

Results and discussion

In order to investigate the gas-sensing properties of the tellurene device, we exposed the device to ~1 ppm of NO_2 in N_2 for three cycles, as shown in **Figure 2a**. The test set-up used for the sensing experiments is shown in **Figure S5**. The exposure time is 240 s every time and then the pure N_2 was injected for 1500 s to flush the chamber. The tellurene sensor responds sensitively when it is switched from pure N_2 to ~1 ppm NO_2. The response is as high as ~122%. **Figure 2b** demonstrated the baseline noise features of the tellurene based chemiresistive sensor. It is evident that the baseline noise is as low as ~0.5%, which is significantly lower than that of phosphorene (~2%) and MoS_2 (~1%) based chemiresistor gas sensors reported in the literature.[13] If we define the limit of detection (LOD) as the concentration at which the response is three times of the baseline noise, the LOD of the tellurene based device is of the order of few tens of ppb toward NO_2 in N_2. This LOD is comparable with the sensitivity of phosphorene based chemiresistive gas sensors.[11] It should be noted that the thickness of tellurene synthesized in this work is distributed from 30 nm to 80 nm. The device sensitivity is expected to increase as the number of 2D layers in the flake is reduced.[11] Therefore, we expect that the sensitivity of such tellurene based chemiresistors (which have already been demonstrated to be excellent in our work), could be even further improved by reducing the flake thickness.

Good repeatability and low baseline drift are important for practical applications of gas sensors. As shown in **Figure 2a**, the

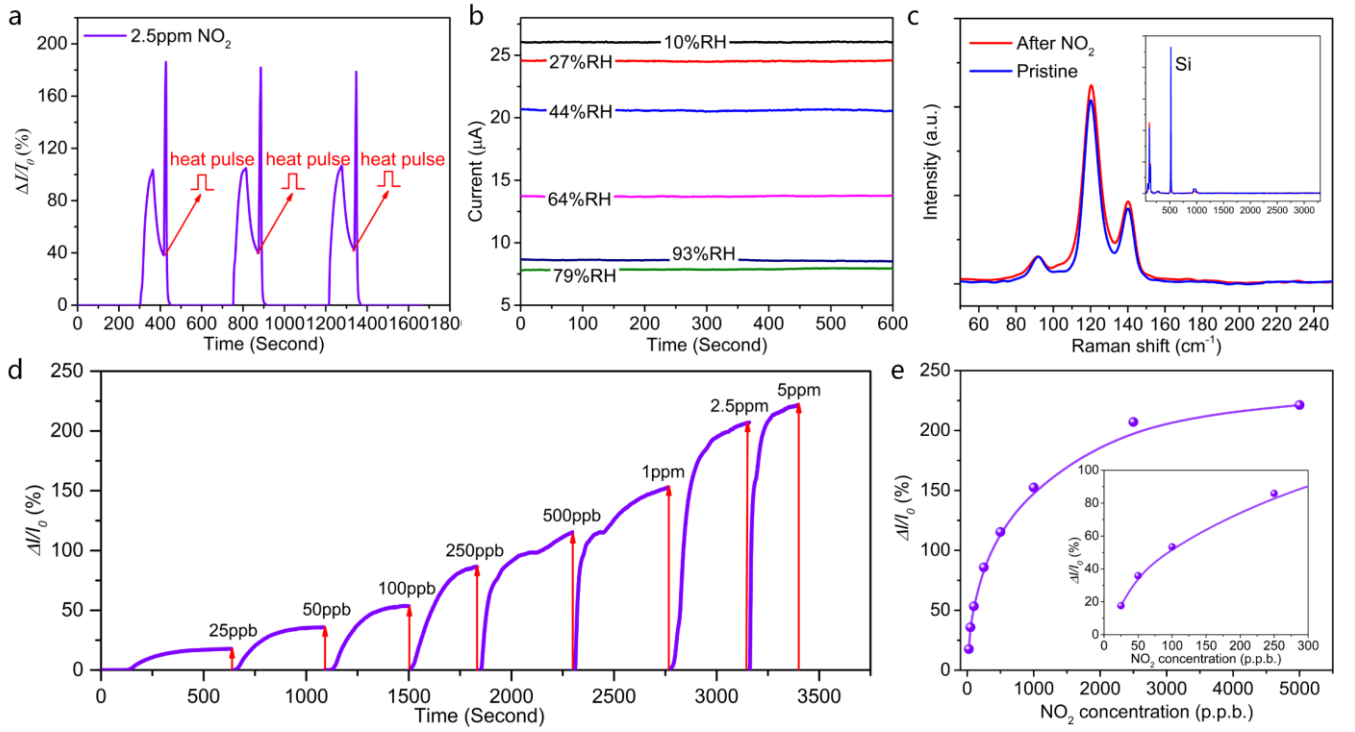

Fig 3. NO_2 gas-sensing properties of the tellurene sensor assisted with a heat pulse: **a**. The response variation behavior versus time with repeated injection of ~2.5 ppm NO_2; b. The current of the tellurene device under different humidity; **c**. Raman spectra of the tellurene sensor before (red) and after (red) exposure to 2.5 ppm NO_2 for 30 min. **d**. Time dependent gas-sensing response toward NO_2 with various concentrations; **e**. The sensor response as a function of gas concentration.

amplitude of response with gas cycling is very similar and the baseline drift is also acceptable. The selectivity of gas sensors is another critical factor because in practical applications, the target gas is usually mixed with other extraneous gas species. To investigate the selectivity of the tellurene device toward NO_2, we chose CO and SO_2 as interference gases because SO_2, CO, and NO_2 are the three main gases associated with air pollution.[31] The dynamic sensing response of the tellurene sensor towards 1 ppm NO_2 mixed with 100 ppm CO and 100 ppm SO_2 were demonstrated in **Figure 2c**. It is evident that the maximum response to NO_2 (with and without mixing with CO) remains almost the same. In fact, the recovery speed improves in the presence of CO, which is advantageous for the sensor. A similar phenomenon is also observed when ~1 ppm NO_2 is mixed with ~100 ppm of SO_2. The only difference being that the recovery speed slows down slightly when NO_2 is mixed with SO_2. These findings indicate that the tellurene based chemiresistive gas sensor is highly selective to NO_2 as compared with CO and SO_2. This is evident based on the fact that even though the concentration of CO or SO_2 is as high as 100 times that of NO_2, the sensor response to NO_2 is only minimally affected by the presence of CO or SO_2. In previous studies, such selectivity tests were usually executed by testing the response of different gases separately.[11, 13, 15] This neglects possible synergistic effects and cross-talk that may arise when gases are mixed together. Therefore, in this work, to better mimic a practical situation, we chose to physically mix NO_2 with CO and SO_2, rather than test the individual gas components separately. The sensor remains highly selective to NO_2, even in the presence of H_2S, NH_3, acetone and ethanol (see **Figure 2d)**. In addition, tellurene exhibits excellent air-stability (**Figure 2e**), and we do not observe any significant change in the sensor's dynamic response (**Figure 2f**) even after 30 days of exposure to air (at ~25°C and ~50% relative humidity).

The one obvious disadvantage of the tellurene sensor is that the recovery times (**Figure 2a**) are as long as thousands of seconds, for ~1 ppm NO_2. In order to improve the recovery speed, we explored the use of heat pulses to assist the recovery process. For this, a substrate with an additional heating electrode was implemented (**Figure S4**). The response variation behaviour versus time with repeated injection of ~2.5 ppm NO_2 is shown in **Figure 3a**. With the help of one single ~10 s long heating pulse, the recovery time was reduced from thousands of seconds to few tens of seconds. Importantly, the heat pulse does not damage the sensor and the response is completely In this way, by properly adjusting the amplitude and duration time of the heat pulses, the recovery time of the tellurene device can be reduced by orders of magnitude. It should be noted that in our case, the heat pulse is only implemented when the sensor has finished responding to the gas. Consequently, the power consumption is acceptable for practical applications, which is very different from traditional semiconducting metal-oxide sensors that reproducible over multiple sensing cycles. require continuous (constant) heating in order to achieve the required sensitivity.[32] The gas response test with "heat pulsing" toward various NO_2 concentrations was also implemented as shown in **Figure 3d**. The lowest concentration that we tested in this experiment is as low as ~25 ppb of NO_2, which further confirms the outstanding chemical sensing performance of tellurene. The sensor response as a function of gas concentration is

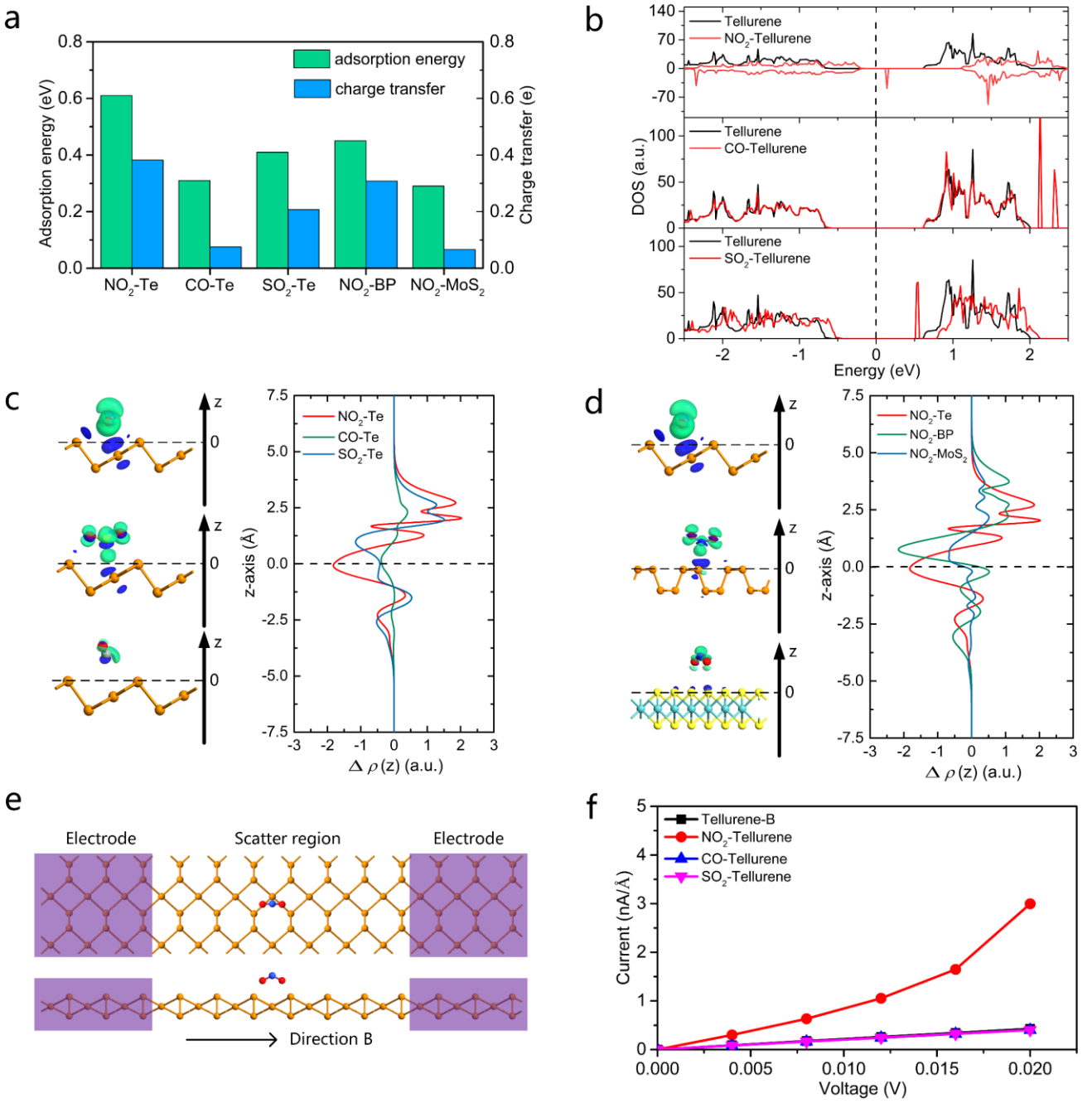

Fig. 4 Results of theoretical study implemented using first principles DFT calculation combined with NEGF method: **a**. Adsorption energy and charge transfer of gas molecules adsorbed on tellurene (Te), phosphorene (BP), and MoS_2. **b**. Density of states (DOS) of tellurene with gas molecules adsorption. **c**. The differential charge density (DCD) isosurface (value: 0.001 e/Å^3) and the averaged one-dimensional charge density change $\Delta\rho(z)$ per area along the x-y plane of the tellurene gas adsorption system. The location of the top layer atoms of the 2D materials is set to be z = 0. **d**. The DCD isosurface (value: 0.001 e/Å^3) of NO_2 adsorption on various 2D material systems and the averaged one-dimensional charge density change $\Delta\rho(z)$ per area along the x-y plane of these systems. **e**. The transport model with two probes along the direction B. The purple shaded region represents the electrode region and the electrodes are heavily p-type doped to improve the convergence. **f**. The predicted current-voltage (*I-V*) curves of tellurene with different gas adsorption along the direction B.

summarized in **Figure 3e**. The rate of change of the sensor response slows down significantly when the NO_2 concentration exceeds ~1 ppm (upper detection limit) due to the saturation of gas adsorption on the tellurene surface. The effect of the humidity was investigated in **Figure 3b**. In the gas sensing tests, the tellurene based sensor demonstrated a p-type semiconductor characteristic. So the current increased under exposure to NO_2 (oxidizing gas) and decreased under exposure to NH_3 and H_2O (reducing gas). In order to investigate the effect of NO_2 exposure to the tellurene sensor, we compared the Raman spectra of tellurene flakes before and after NO_2 exposure in **Figure 3c**. The Raman peaks (E_1 at 91.4 cm^{-1}, A_1 at 119.0 cm^{-1} and E_2 at 139.2 cm^{-1}) of pristine tellurene remained in the same positions and the relative intensity was also nearly the same. This indicates that NO_2 exposure induces minimal chemical degradation of the tellurene flakes.

In order to gain fundamental insight into the underlying mechanism(s) for the sensing performance of tellurene, we performed first principles calculation combined with the non-equilibrium Green's functions (NEGF) method to investigate the gas sensing performance of tellurene.[33] The computational details of the simulation are explained in the Methods Section. We used the slab model to simulate the surface of 2D materials and a vacuum distance of 15 Å was used to avoid the influence of mirror images caused by periodic boundary conditions. The optimized adsorption structure of gas adsorbed on various 2D materials are displayed in **Figure S6**. We defined the adsorption energy as follows: E_{ads} = E(Gas) + E(2D Material) − E(Gas+2D Material). Bader analysis was performed to estimate the charge transfer value of gas molecules adsorbed on 2D materials.[34] In **Figure 4a**, we show the adsorption energy and charge transfer of different adsorption systems: NO_2 adsorbed on tellurene (Te), CO adsorbed on Te, SO_2 adsorbed on Te, NO_2 adsorbed on phosphorene (BP), and NO_2 adsorbed on MoS_2. We find that the NO_2 molecule (on tellurene) has both the largest adsorption energy and the largest charge transfer value when compared with the CO molecule and the SO_2 molecule on tellurene. This indicates that the NO_2 molecule has the strongest interaction with tellurene. Interestingly, the adsorption energy and charge transfer value of NO_2 adsorbed on tellurene are also larger than these of NO_2 adsorbed on phosphorene and MoS_2. For a visual description of charge transfer between gas molecules and tellurene and a comparison with adsorption on other 2D materials, such as phosphorene and MoS_2, we plotted the differential charge density (DCD) isosurface and the averaged one-dimensional charge density change $\Delta\rho(z)$ per area along the x-y plane of the gas adsorption system in **Figure 4c** and **Figure 4d**. For NO_2, CO, and SO_2 adsorption on tellurene, the amplitude of NO_2 $\Delta\rho(z)$ curve is significantly larger than those of CO and SO_2, which is consistent with the larger DCD isosurface of the NO_2 adsorption system. Therefore, we can conclude that the charge redistribution associated with NO_2 adsorption on tellurene is very intense, which explains the high sensitivity and high selectivity of tellurene to NO_2. The amplitude of NO_2 adsorption on tellurene ($\Delta\rho(z)$) is much larger than that of NO_2 adsorption on MoS_2 and is similar to that of NO_2 adsorption on phosphorene. This explains why the sensitivity of tellurene toward NO_2 is greater than MoS_2, but similar to that of phosphorene.

Next, we investigated the effects of gas adsorption on the electronic properties of tellurene. We show the density of states (DOS) of tellurene with adsorption of NO_2, CO, and SO_2 in **Figure 4b**. A high level of doping of tellurene was observed with the adsorption of NO_2. The fermi level of tellurene moved from the middle of the gap to the valence band, indicating that NO_2 adsorption induces a heavy p-type doping of tellurene. Therefore, NO_2 adsorption significantly changes the electronic properties of tellurene. On the contrary, the adsorption of CO induces a very slight shift of the fermi level of tellurene and the shift induced by SO_2 adsorption is also much smaller than that of NO_2 adsorption. The DOS of NO_2 adsorption on phosphorene and MoS_2 are shown in **Figure S7**. The results indicate that the adsorption of NO_2 induces a significant shift of the fermi level for all three categories of 2D materials (tellurene, phosphorene, and MoS_2) considered here. All the three 2D materials are therefore sensitive to NO_2. Resistance change is a critical maker for chemiresistor-type gas sensors, and electronic transport calculations can simulate the current-voltage relation before and after gas adsorption [35]. To study this, we built a transport model with two probes where semi-infinite left and right electrode regions (purple shaded region) are in contact with the central scattering region. The electrodes are heavily p-type doped to improve the convergence. Due to the structural anisotropy of tellurene, we built two transport models: one has current flowing along the direction A (in **Figure S8**), and the other has the current flowing along the direction B as shown in **Figure 4e**. **Figure 4f** demonstrates the current-voltage relation of tellurene before and after the gas adsorption. It is evident that NO_2 adsorption induces a very substantial change of the current-voltage relation of tellurene. On the contrary, CO and SO_2 adsorption does not significantly affect the current-voltage relation. Therefore, NO_2 adsorption induces a significant resistance change to tellurene, while CO and SO_2 adsorption does not, which is consistent with our experimental observations.

Sensing performance of typical 2D materials toward NO_2 are listed in **Table 1**. Tellurene offers an outstanding LOD for NO_2 detection of ~25 ppb. Though phosphorene has a LOD of ~5 ppb toward NO_2, a critical difficulty hindering its practical application is its limited air-stability.[20] In contrast, the air stability of tellurene have been confirmed by different research groups experimentally and theoretically.[21, 22, 26, 36] To verify this, we exposed tellurene to air at ~25 ℃ and ~50% relative humidity (RH) for 30 days to establish its air-stability. The Raman spectra of tellurene before and after exposure to air for 30 days has been displayed in **Figure 2e**. No peak shift or new peaks were observed which indicated that tellurene remained stable in air. Furthermore, we also performed a sensing test of the tellurene sensor after exposure to the air for 30 days as shown in **Figure 2f**. No distinct change of dynamic sensing response was found. Tellurene also offers a much wider detection range (**Table 1**) as compared to phosphorene and other 2D materials. It should be noted that the human exposure limit to NO_2 is 53 ppb according to the U.S. Government's Environmental Protection Agency.[37] Evidently, for MoS_2, SnS_2 and rGO, the LODs (**Table 1**) toward NO_2 are higher than the limit level. Moreover, the high operating temperatures of SnS_2 and rGO results in high energy consumption, which is another important factor that favors the deployment of tellurene in chemiresistive sensor devices.

Table 1. Sensing performance of typical 2D materials toward NO_2.

Channel material	Limit of detection	Detection range	Operation temperature	Air stability	Reference

Tellurene	~25 ppb	25 ppb to 5 ppm	room temperature	excellent	this work
Phosphorene	~5 ppb	5 ppb to 40 ppb	room temperature	poor	[10]
MoS_2	~100 ppm	100 ppm to 1000 ppm	room temperature	good	[38]
SnS_2	~0.6 ppm	0.6 ppm to 10 ppm	~120 ℃	excellent	[39]
rGO	~100 ppb	100 ppb to 8 ppm	~60 ℃	excellent	[40]

Conclusions

In summary, we have investigated 2D tellurene based devices for chemical sensing. Gas sensors based on tellurene achieved a LOD of ~25 ppb to NO_2, which is superior to MoS_2, SnS_2 and rGO based devices. While phosphorene-based sensors offer a similar detection limit, tellurene exhibits excellent air-stability, while phosphorene does not. Tellurene also offers a superior detection range (25 ppb to 5 ppm) for NO_2 sensing. Another key attribute of tellurene is that it is highly selective to NO_2 detection and experiences minimal cross-contamination when exposed to other common air pollutants such as CO, SO_2, H_2S, NH_3, acetone and ethanol. The baseline noise of tellurene sensing devices is about 0.5%, which is significantly lower than that of phosphorene and MoS_2. In addition, we find that heat pulsing is an effective strategy to improve the recovery speed of tellurene. First-principles ab initio calculations demonstrated that large adsorption energy and intense charge redistribution takes place when NO_2 interacts with tellurene, which explains the high sensitivity and selectivity of tellurene to NO_2. To our knowledge, this is the first experimental report detailing the chemical sensing possibilities of tellurene. Until now tellurene has mainly been studied for its electronics and optoelectronics applications. This work could open new vistas for this exciting new material in the arena of chemical (gas) sensing.

Conflicts of interest

There are no conflicts to declare.

Acknowledgements

This work was supported by National Key Basic Research Program of China (973 Program) (2015CB251001), National Natural Science Foundation of China (No.51877170), Young Elite Scientists Sponsorship Program by CAST, and the Fundamental Research Funds for the Central Universities. The calculations in this work were carried out on the HPC Platform, Xi'an Jiaotong University, and Tianhe-2 in the Lvliang Supercomputer Center. NK acknowledges support from the USA National Science Foundation (Award 1608171) and the John A. Clark and Edward T. Crossan Chair Professorship at the Rensselaer Polytechnic Institute, USA.

Notes and references

1 F. Schedin, A. K. Geim, S. V. Morozov, E. W. Hill, P. Blake, M. I. Katsnelson and K. S. Novoselov, NAT MATER, 2007, 6, 652.
2 A. K. Geim and K. S. Novoselov, NAT MATER, 2007, 6, 183-191.
3 B. Radisavljevic, A. Radenovic, J. Brivio, V. Giacometti and A. Kis, NAT NANOTECHNOL, 2011, 6, 147-150.
4 M. Naguib, O. Mashtalir, J. Carle, V. Presser, J. Lu, L. Hultman, Y. Gogotsi and M. W. Barsoum, ACS NANO, 2012, 6, 1322-1331.
5 D. Wang, X. Wang, A. Yang, J. Chu, P. Lv, Y. Liu and M. Rong, IEEE ELECTR DEVICE L, 2018, 39, 292-295.
6 A. Yang, D. Wang, X. Wang, J. Chu, P. Lv, Y. Liu and M. Rong, IEEE ELECTR DEVICE L, 2017, 38, 963-966.
7 S. Zhang, Z. Yan, Y. Li, Z. Chen and H. Zeng, ANGEW CHEM INT EDIT, 2015, 54, 3112-3115.
8 S. Zhang, S. Guo, Z. Chen, Y. Wang, H. Gao, J. Gómez-Herrero, P. Ares, F. Zamora, Z. Zhu and H. Zeng, CHEM SOC REV, 2018, 47, 982-1021.
9 D. Chen, X. Zhang, H. Cui, J. Tang, S. Pi, Z. Cui, Y. Li and Y. Zhang, APPL SURF SCI, 2019, 479, 852-862.
10 A. N. Abbas, B. L. Liu, L. Chen, Y. Q. Ma, S. Cong, N. Aroonyadet, M. Kopf, T. Nilges and C. W. Zhou, ACS NANO, 2015, 9, 5618-5624.
11 S. M. Cui, H. H. Pu, S. A. Wells, Z. H. Wen, S. Mao, J. B. Chang, M. C. Hersam and J. H. Chen, NAT COMMUN, 2015, 6.
12 K. Lee, R. Gatensby, N. McEvoy, T. Hallam and G. S. Duesberg, ADV MATER, 2013, 25, 6699-6702.
13 S. J. Kim, H. J. Koh, C. E. Ren, O. Kwon, K. Maleski, S. Y. Cho, B. Anasori, C. K. Kim, Y. K. Choi, J. Kim, Y. Gogotsi and H. T. Jung, ACS NANO, 2018, 12, 986-993.
14 X. H. Liu, T. T. Ma, N. Pinna and J. Zhang, ADV FUNCT MATER, 2017, 27.
15 J. Chu, X. Wang, D. Wang, A. Yang, P. Lv, Y. Wu, M. Rong and L. Gao, CARBON, 2018, 135, 95-103.
16 Z. Cui, X. Zhang, D. Chen and Y. Tian, APPL SURF SCI, 2019, 483, 409-416.
17 D. Zhang, M. Wang and Z. Yang, Sensors and Actuators B: Chemical, 2019, 292, 187-195.
18 D. Zhang, Z. Wu and X. Zong, Sensors and Actuators B: Chemical, 2019, 289, 32-41.
19 J. Dai, T. Zhang, H. Zhao and T. Fei, SENSOR ACTUAT B-CHEM, 2017, 242, 1108-1114.
20 A. J. Yang, D. W. Wang, X. H. Wang, D. Z. Zhang, N. Koratkar and M. Z. Rong, NANO TODAY, 2018, 20, 13-32.
21 Y. X. Wang, G. Qiu, R. X. Wang, S. Y. Huang, Q. X. Wang, Y. Y. Liu, Y. C. Du, W. A. Goddard, M. J. Kim, X. F. Xu, P. D. Ye and W. Z. Wu, NATURE ELECTRONICS, 2018, 1, 228-236.
22 W. Z. Wu, G. Qiu, Y. X. Wang, R. X. Wang and P. D. Ye, CHEM SOC REV, 2018, 47, 7203-7212.
23 X. H. Wang, D. W. Wang, A. J. Yang, N. Koratkar, J. F. Chu, P. L. Lv and M. Z. Rong, PHYS CHEM CHEM PHYS, 2018, 20, 4058-4066.
24 Z. L. Zhu, X. L. Cai, S. H. Yi, J. L. Chen, Y. W. Dai, C. Y. Niu, Z. X. Guo, M. H. Xie, F. Liu, J. H. Cho, Y. Jia and Z. Y. Zhang, PHYS REV LETT, 2017, 119.
25 J. L. Chen, Y. W. Dai, Y. Q. Ma, X. Q. Dai, W. K. Ho and M. H. Xie,

NANOSCALE, 2017, 9, 15945-15948.
26 Y. X. Wang, R. Ferreira, R. X. Wang, G. Qiu, G. D. Li, Y. Qin, P. Ye, A. Sabbaghi and W. Z. Wu, NANO ENERGY, 2019, 57, 480-491.
27 S. J. Yang, B. Chen, Y. Qin, Y. Zhou, L. Liu, M. Durso, H. L. Zhuang, Y. X. Shen and S. Tongay, PHYS REV MATER, 2018, 2.
28 S. Y. Cho, Y. Lee, H. J. Koh, H. Jung, J. S. Kim, H. W. Yoo, J. Kim and H. T. Jung, ADV MATER, 2016, 28, 7020.
29 A. Castellanos-Gomez, M. Buscema, R. Molenaar, V. Singh, L. Janssen, H. van der Zant and G. A. Steele, 2D MATER, 2014, 1.
30 H. W. Chen, Y. T. Chen, H. Zhang, D. W. Zhang, P. Zhou and J. Huang, ADV FUNCT MATER, 2018, 28.
31 C. Song, L. Wu, Y. Xie, J. He, X. Chen, T. Wang, Y. Lin, T. Jin, A. Wang and Y. Liu, ENVIRON POLLUT, 2017, 227, 334-347.
32 A. P. Lee and B. J. Reedy, Sensors and Actuators B: Chemical, 1999, 60, 35-42.
33 S. Datta, SUPERLATTICE MICROST, 2000, 28, 253-278.
34 W. Tang, E. Sanville and G. Henkelman, J PHYS-CONDENS MAT, 2009, 21.
35 L. Kou, T. Frauenheim and C. Chen, The journal of physical chemistry letters, 2014, 5, 2675-2681.
36 X. Ren, Y. Wang, Z. Xie, F. Xue, C. Leighton and C. D. Frisbie, NANO LETT, 2019.
37 https://www.epa.gov/, 2019.
38 D. J. Late, Y. Huang, B. Liu, J. Acharya, S. N. Shirodkar, J. Luo, A. Yan, D. Charles, U. V. Waghmare and V. P. Dravid, ACS NANO, 2013, 7, 4879-4891.
39 J. Z. Ou, W. Ge, B. Carey, T. Daeneke, A. Rotbart, W. Shan, Y. Wang, Z. Fu, A. F. Chrimes and W. Wlodarski, ACS NANO, 2015, 9, 10313-10323.
40 Y. Zhou, G. Liu, X. Zhu and Y. Guo, Sensors and Actuators B: Chemical, 2017, 251, 280-290.

